Independent isomer yield ratio of ^{90}Rb from thermal neutron fission of ^{235}U

P. L. Reeder and R. A. Warner
Pacific Northwest Laboratory, Richland, Washington 99352

G. P. Ford
Los Alamos National Laboratory, Los Alamos, New Mexico 87545

H. Willmes
University of Idaho, Moscow, Idaho 83843

(Received 28 May 1985)

The independent isomer yield ratio for ^{90}Rb from thermal neutron fission of ^{235}U has been measured by use of a new technique involving a pulsed reactor and an on-line mass spectrometer facility. The apparent isomer yield ratio was measured for several ion collection time intervals of different durations and extrapolated to zero collection time to eliminate interference from ^{90}Kr decay. The observed independent isomer yield ratio of 8.7 ± 1.0 for $(^{90}\mathrm{Rb}^{m})/^{90}\mathrm{Rb}^{g})$ is one of the largest ratios measured for a low energy fission process. However, a statistical model analysis shows that the average angular momentum ($\langle J\rangle=4.5$) deduced from this isomer yield ratio is consistent with average angular momentum for several other products from low energy fission.

INTRODUCTION

It has long been known that fission fragments have greater nuclear spin than that of the initial fissioning system. The angular momentum induced by the fission process has been attributed to Coulomb forces acting on nonaxially symmetric scission configurations and to bending and wriggling modes of collective excitation.[1–4] An alternative model by Fong based on statistical theory suggests that the angular momentum is generated by excitation of single particles.[5] The available experimental data on angular momentum of the primary fragments do not entirely exclude either approach.[6]

One technique for determining the primary fragment angular momentum is the measurement of the relative population of different members of the ground state rotational band of an even-even fission product.[7] Another method is the measurement of the number of gamma rays emitted by the fission fragments.[8] The anisotropy of specific gamma rays relative to the fragment direction has also been used.[7,9,10] However, the most frequently used technique is the measurement of independent isomer yield ratios. A summary of experimental results for fission fragments was published by Aumann *et al.* in 1977.[11] More recent results from radiochemical techniques are given in Refs. 6 and 12–17.

Radiochemical measurements of independent isomer yield ratios require a chemical separation of the element of interest in a time which is very short compared to beta decay of the precursor nuclide. About 19 fission product nuclides have been measured by this technique. The on-line recoil mass separator LOHENGRIN has permitted measurements of isomer yield ratios for additional nuclides including isomers with μs half-lives.[18,19] These on-line measurements give considerably more information because the isomer yield ratio can be measured as a function of the excitation energy of the initial fragment.

The present work describes a new technique for measuring isomer yield ratios which uses a pulsed reactor in conjunction with an on-line mass spectrometer. This technique is potentially more versatile than the standard radiochemical technique in that yields of nuclides with half-lives as short as a few seconds can be measured. It does not provide the excitation energy dependence as does the recoil mass separator technique. In the following sections, we describe the technique, give the results of measurements on ^{90}Rb, and discuss the conversion of the isomer yield ratio to the average angular momentum of the fission product by use of the statistical model of Ford *et al.*[17]

EXPERIMENTAL METHODS

These experiments were performed at Pacific Northwest Laboratory's Spectrometer for On-Line Analysis of Radionuclides (SOLAR) facility located at the Nuclear Radiation Center of Washington State University.[20] The floor plan of the SOLAR facility is shown in Fig. 1. The reactor normally operates at a steady state power level of 1 MW. For this work, the reactor was operated in pulsed mode with pulses up to 1000 MW with FWHM of 10 ms.

The ^{235}U target was located in the thermal column with 56 cm of graphite between the core and the target. The thermal neutron flux at the target under steady state power was about 6×10^{10} n/cm^{2}s with a Cd ratio for Au flux wires of about 20. The target consisted of about 0.3 g of 93% enriched ^{235}U mixed with graphite powder and pressed into a pellet about 0.63 cm diam by 0.9 cm long. The target was contained in a Ta oven which was heated to about 1600 °C by electron bombardment.

Fission product Rb and Cs nuclides diffuse rapidly

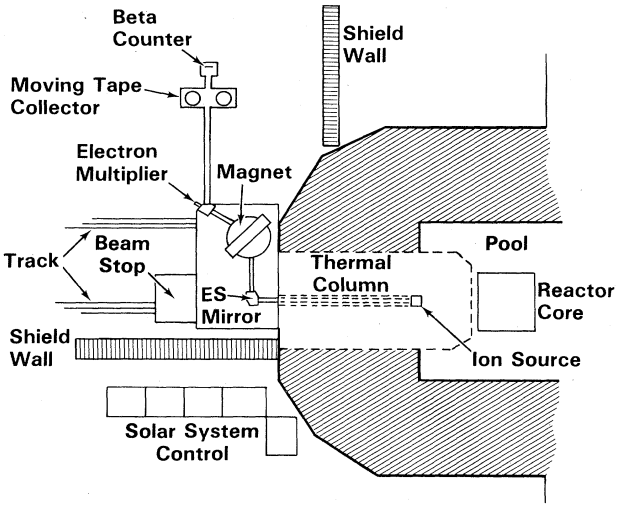

FIG. 1. Floor plan of SOLAR facility.

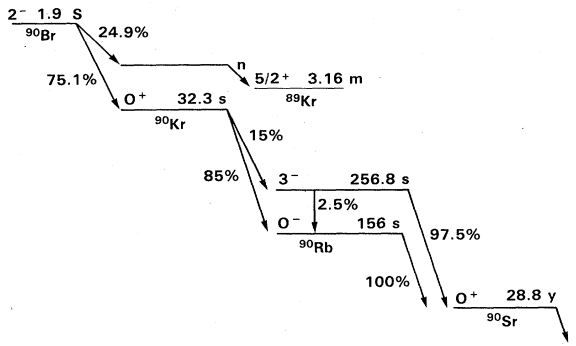

FIG. 2. Outline of mass 90 decay chain.

from the U/graphite target and are efficiently ionized on the hot Ta surface. Neighboring elements are not ionized under these conditions. The mass spectrometer selects only the mass number of interest so chemically and mass separated nuclides are delivered to the collection point.

For the independent isomer yield ratio measurements, it is necessary to collect the nuclide of interest in a time that is short compared to the lifetime for decay of the preceding isobar in the mass chain. The reactor is pulsed to produce a large number of fission products in the target at a known time. Fission product ions at the desired mass are collected for a short time interval during and after the reactor pulse. After the ion beam is switched off, the decay of the two isomers is measured by beta and/or gamma counting. The relative amounts of the two isomers determined by the decay data gives the isomer yield ratio for the particular collection time chosen. The isomer yield ratio is measured for several ion beam collection times and the isomer yield ratio is extrapolated to zero collection time.

The first nuclide studied by this technique was ^{90}Rb. The pertinent features of the mass 90 decay chain are shown in Fig. 2. Early decay scheme studies suggested 1^- and 4^- for the spin/parity of the ground and metastable isomers[21] but recent work gives 0^- and 3^-.[22,23] The gamma intensity of the isomeric transition is $(0.20\pm0.04)\%$ of the ^{90}Rb^m decays.[21,23] The total conversion coefficient from Ref. 21 is 11.5 ± 0.9, which gives a branching fraction of $(2.5\pm0.5)\%$ for the isomeric transition. This branching fraction has a small influence on the analysis of the beta decay curves discussed below. The branching fractions of ^{90}Kr to the two ^{90}Rb isomers is taken from Ref. 23. The beta-delayed neutron branching fraction for ^{90}Br is from the compilation by Mann *et al.*[24] These fractions are important in the analysis of the isomer yield ratio versus ion collection time data.

From Rider's compilation of fission yield data,[25] the ratio of the ^{90}Kr independent fission yield to the ^{90}Rb^{m,g} independent fission yield is 5.2. Because the ^{90}Kr yield is so much greater than the ^{90}Rb yield and because most of the ^{90}Kr decays to the ground state isomer, the apparent isomer yield ratio is strongly dependent on the amount of ^{90}Kr decay during the ^{90}Rb ion collection time. In our analysis of the isomer yield ratio versus ion collection time data we allow the independent yields of the ^{90}Kr, ^{90}Rb^m, and ^{90}Rb^g to be unknown quantities and determine all three by a least squares fit to the data. We thus obtain both the ^{90}Rb isomer yield ratio and the ratio of ^{90}Kr independent yield to ^{90}Rb^{m,g} independent yield from the same experiments.

The beta counter used in this work was a transmission mounted Si surface barrier detector 1000 μm thick with an area of 450 mm^2. One series of experiments was done with the beta counter off line in a well-shielded cave. The ^{90}Rb was collected on an Al foil disk mounted on a vacuum interlock at the location of the electron multiplier in Fig. 1. Immediately after the ion collection period, the foil was removed from the vacuum interlock and mounted in front of the beta counter. Transfer of the sample took 30—40 s. The beta multiscalar was started simultaneously with the neutron burst and continued for at least eight half-lives of the longer-lived isomer. Another series of measurements was done with the beta counter mounted on line as shown in Fig. 1. The ion beam was deposited on an aluminized Mylar tape in front of the detector. The tape was stationary during collection and counting, but it was moved before the next reactor burst. A thick Al collimator was mounted at the entrance to the beta counter vacuum box to ensure that no ion beam missed the 1.27 cm wide tape. Even though the on-line beta counting eliminated the transfer delay, the ion collection and beta counting were less efficient so that the statistical accuracy of the beta decay curve analysis was equivalent for the on-line and off-line experiments.

The beta decay curves were analyzed with the least-square fitting code MASH.[26] An example of a beta decay curve taken on line is shown in Fig. 3. The beta activity is dominated by the ^{90}Rb^m and ^{90}Rb^g components. However there is a small component due to the growth of ^{90}Rb^g from the isomeric transition. In addition there was a short-lived background component ($t_{1/2}=2.8\pm0.5$ s). This component was observed after the neutron pulse even when the ion beam was brought out to the electron multiplier but not sent down to the beta counter. This background is probably due to neutral gaseous activity. It was minimized by placing baffles before the bending magnet

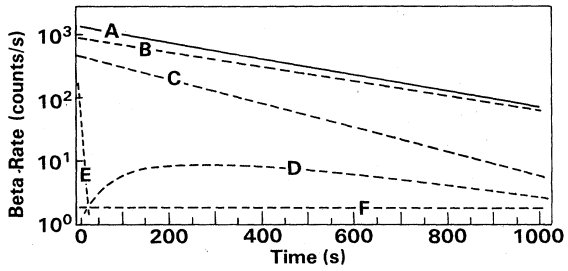

FIG. 3. Typical beta decay curves of ^{90}Rb after a single neutron pulse and ion collection for 5 s: Experimental data taken on line (*A*); ^{90}Rb^m, $t_{1/2}=256.8$ s (*B*); ^{90}Rb^g, $t_{1/2}=156$ s (*C*); ^{90}Rb^g from isomeric transition from ^{90}Rb^m (*D*); background, $t_{1/2}=2.8$ s (*E*); background, $t_{1/2}=\infty$ (*F*).

and at the electron multiplier box and by doing differential pumping. The long-lived background was about 0.2 cps in the off-line counting arrangement and about 10 times greater in the on-line configuration. The data shown in Fig. 3 were from a single neutron burst. Only at the shortest ion collection times (0.3 and 0.5 s) was it necessary to combine decay curves from several pulses to get sufficient statistical accuracy.

To measure the isomer yield ratio by beta counting, it is important that the beta counting efficiency be the same for both isomers. The transmission beta counter used in this work does not give a pulse height spectrum proportional to the beta energy since high energy betas pass completely through the detector. The beta pulse height spectrum from ^{90}Rb is shown in Fig. 4. The beta spectra from sources of ^{90,92,94}Rb were compared and were found to be almost identical except for the height of the valley. All these nuclides have beta decay Q values of greater than 6 MeV, so one expects most of the betas to deposit the same amount of energy, which would be about 350 keV for the 1000 μm thick Si detector. The broad peak in Fig. 4 centered about channel 55 was about 280 keV based on a calibration with a ^{207}Bi conversion electron source. The maximum beta energy which is completely stopped in the detector is about 700 keV. The pulse height spectrum indicates that most of the beta pulses are due to minimum ionizing betas, i.e., greater than 1 MeV. The discriminator was set in the valley region which was about 100 keV.

It is possible that some of the pulses in the valley region

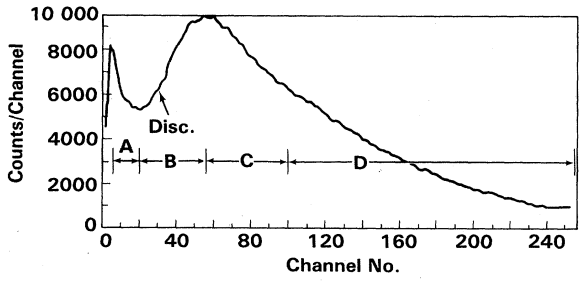

FIG. 4. ^{90}Rb pulse height spectrum in Si beta counter for beta multispectrum scaling experiment. Isomer yield ratio was determined for each of the four regions *A*–*D*. The discriminator setting for the normal beta multiscaling experiments is indicated.

are due to gamma rays or x rays, particularly for ^{90}Rb which had the lowest peak to valley ratio of the three Rb isotopes. We therefore performed a beta multispectrum scaling experiment in which the beta spectrum from ^{90}Rb was measured as a function of time after the neutron burst. The beta spectrum was divided into four regions as shown in Fig. 4 and the isomer yield ratio was determined for each pulse height region. If the beta counting efficiency is the same for both isomers, the isomer yield ratio should be the same for all pulse height regions. The regions labeled *B*, *C*, and *D* in Fig. 4 all gave the same isomer yield ratio within the statistical uncertainties. Region *A* had a significantly higher isomer yield ratio indicating an enhanced efficiency for detecting ^{90}Rb^m. However this pulse height region contains events other than true beta pulses as shown by a spectrum taken with a thick absorber in front of the detector. We assumed that pulses above the discriminator were true beta pulses and were equally efficient for ^{90}Rb^m and ^{90}Rb^g.

RESULTS

The least square fitting code MASH gave the number of atoms of each component present at the initial time (which was assumed to be the maximum of the neutron flux). The ^{90}Rb^g due to the isomeric transition from ^{90}Rb^m (*D*, Fig. 3) was added to the ^{90}Rb^m (*B*, Fig. 3) to get the total ^{90}Rb^m. This total was divided by the number of atoms of ^{90}Rb^g (*C*, Fig. 3) to give the apparent isomer yield ratio (high-spin yield/low-spin yield) for the particular ion collection time. The results are listed in Table I and plotted in Fig. 5. In the analysis given below, no distinction was made between data obtained by off-line or on-line beta counting.

To obtain the isomer yield ratio at zero ion collection time, we derived an analytical expression for the diffusion and decay of all the members of the mass 90 decay chain. We first define the rate of change of each component within the oven/target.

$$\frac{dQ}{dt}=-(\lambda_K^Q+\lambda_D^Q)Q\ , \tag{1}$$

$$\frac{dP}{dt}=\lambda_K^Q Q-(\lambda_K^P+\lambda_D^P)P\ , \tag{2}$$

$$\frac{dM}{dt}=f^M\lambda_K^P P-(\lambda_K^M+\lambda_D^M)M\ , \tag{3}$$

$$\frac{dG}{dt}=(1-f^M)\lambda_K^P P-(\lambda_K^G+\lambda_D^G)G\ , \tag{4}$$

where Q is the number of atoms of grandparent (^{90}Br); P is the number of atoms of parent (^{90}Kr); M is the number of atoms of metastable isomer (^{90}Rb^m); G is the number of atoms of ground state isomer (^{90}Rb^g); λ_K^i is the radioactive decay rate constant for $i=Q$, P, M, or G; λ_D^i is the diffusion rate constant for $I=Q$, P, M, or G; and f^M is the fraction of precursor decays which go to metastable isomer.

These differential equations were then solved for M and G. Since only M and G are ionized, the ion deposition rates for M and G are given by

TABLE I. Apparent isomer yield ratio (high spin/low spin) for ^{90}Rb for various ion collection times.

Ion collection time (s)[a]	Isomer yield ratio	Beta counting on line or off line	Number of neutron bursts combined
0.07	9.40±1.07	off	2
0.07	6.56±1.03	on	4
0.27	9.59±0.76	off	1
0.27	6.93±0.98	on	1
0.27	8.40±0.81	on	3
0.77	6.46±0.32	off	1
0.77	6.59±0.71	on	1
1.77	5.21±0.18	off	1
1.77	4.80±0.38	on	1
2.77	4.32±0.11	off	1
2.77	3.87±0.16	on	1
4.77	3.22±0.09	on	1

[a]Actual ion collection time included an additional 0.23 s delay from the time of the trigger signal to the time of the neutron burst.

$$\frac{dM^+}{dt}=\lambda_D^M M\ , \tag{5}$$

$$\frac{dG^+}{dt}=\lambda_D^G G\ . \tag{6}$$

We assume that the ionization efficiencies for the two isomers are equal and cancel since we are only interested in relative ion rates. The number of ions collected is the integral of the ion deposition rate over the ion collection time (t) so the apparent isomer yield ratio is given by

$$\text{IYR}=\frac{\int_0^t \lambda_D^M M\,dt}{\int_0^t \lambda_D^G G\,dt}\ . \tag{7}$$

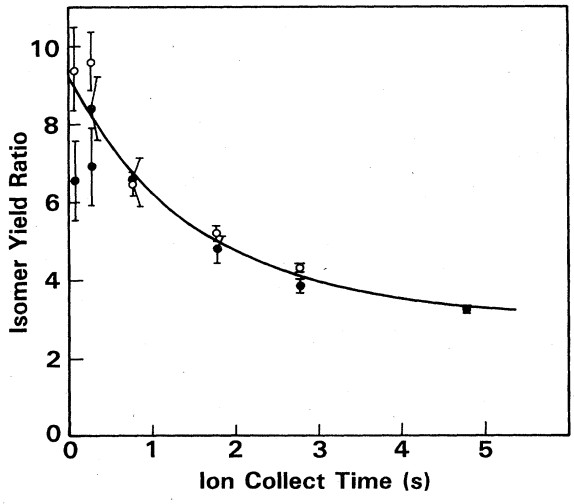

FIG. 5. The apparent isomer yield ratio for ^{90}Rb plotted versus the ion collection time. The solid circles are from on line, the open circles from off line beta counting. The solid curve is the least square fitted curve of the analytical expression for diffusion and decay.

The analytical expression defined by Eq. (7) contains the parameters Q_0, P_0, M_0, and G_0 which are the number of atoms initially present after the neutron burst. A least square fitting code was written to fit the latter three parameters to the experimental data given in Table I. The parameter Q_0 is proportional to the ^{90}Br cumulative fission yield which is 12% of the ^{90}Kr independent yield.[25] To simplify the least square fitting, the ratio of the ^{90}Br cumulative yield to the ^{90}Kr independent yield was held constant throughout the fitting calculation. The ratio actually used was 0.09 to account for the 24.9% delayed neutron branch in the decay of ^{90}Br. The solid line through the data in Fig. 5 is the best fit of Eq. (7) to the data. The independent isomer yield ratio is M_0/G_0. In addition, the ratio of Kr independent yield to Rb independent yield is given by $P_0/(M_0+G_0)$.

Before doing the least square fit, the diffusion rate constants λ_D for Q, P, M, and G must be determined. Previous work has shown that diffusion rate constants for isotopes of a given element are practically the same.[27] There should be even less variation of the diffusion constants between isomers, so we assume that $\lambda_D^M=\lambda_D^G=\lambda_D^{\text{Rb}}$.

The Rb diffusion rate constant was measured by pulsing the reactor and following the disappearance of the Rb ion count rate as a function of time. The ions were detected by the 17 stage electron multiplier located as shown in Fig. 1. To avoid complications from decay of Kr in the oven/target, one would prefer to measure a Rb nuclide for which the Rb fission yield greatly exceeds the Kr fission yield. However, the radioactive half-life of the Rb must be much longer than the Rb diffusion time to avoid complications from Rb decay. We measured Rb diffusion curves at both mass 90 and 91 and obtained

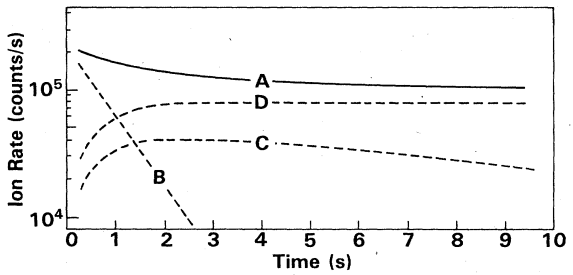

FIG. 6. Ion count rate and fitted components at mass 91 as functions of time after a neutron burst: Experimental data (*A*); ^{91}Rb diffusion from oven, $t_{1/2}=0.55$ s (*B*); ^{91}Rb diffusion following ^{91}Kr decay in oven (*C*); growth and decay of ^{91}Rb beta activity on electron multiplier (*D*).

equivalent results. The ^{91}Rb data are shown in Fig. 6 along with the components fit by the MASH program. We assumed that Rb diffusion was described by a single exponential component. Another component must be included to account for Rb from decay of Kr in the oven/target. The MASH program treats this component as a mother-daughter growth and decay situation where the decay of the mother is not observed and the daughter has the half-life of Rb diffusion. The electron multiplier has some efficiency for detecting beta particles from any radioactive nuclide deposited on the first dynode. However, the efficiency is strongly dependent on the particular nuclide and on the exact location of the deposit on the dynode. Therefore, a third component was included in the diffusion curve analysis which accounted for growth of the Rb daughter from a parent disappearing with the Rb diffusion half-life. The Rb diffusion rate constant is dependent on the temperature of the oven, so all experiments were done at the same temperature, 1600 °C. With our target material and this temperature, the Rb diffusion half-life was 0.55 ± 0.01 s.

The Kr diffusion rate constant (λ_D^P) is not easily measured. Therefore, we did the least square fit of Eq. (7) to the data of Table I for several values of λ_D^P and plotted chi-square per degree of freedom (χ_ν^2) vs λ_D^P to find the minimum. This plot is shown in Fig. 7 along with the corresponding results for the isomer yield ratio and the Kr/Rb fission yield ratio. The minimum χ_ν^2 is for a Kr diffusion time of 2.75 s. The corresponding value for the isomer yield ratio is 8.7 ± 0.3 and the Kr independent yield to Rb independent yield ratio is 4.1 ± 0.2. Although χ_ν^2 does not increase rapidly as one goes to longer Kr diffusion times, the Kr/Rb yield ratio would be even lower for longer λ_D^P and would disagree more with the value of 5.2 recommended by Rider.[25]

The isomer yield ratio is rather insensitive to reasonable variations of the other parameters in the diffusion and decay model, whereas the yield ratio of Kr/Rb is more sensitive. For example, the Br diffusion time was normally fixed at 10^6 s (infinity). Changing the time to 1.9 s increased the isomer yield ratio by less than 0.5% and increased the Kr/Rb yield ratio by 3%. Changing the branching fraction of ^{90}Kr decay to ^{90}Rb^m from 0.15 to 0.20 increased the isomer yield ratio by less than 0.4% and increased the Kr/Rb yield ratio by 8.5%. By simultaneously decreasing the Br diffusion time, increasing the branching fraction of ^{90}Kr decay to ^{90}Rb^m, and increasing the Rb diffusion time, we can raise the Kr/Rb yield ratio to 4.8 without changing the isomer yield ratio or χ_ν^2 significantly. Thus the Kr/Rb yield ratio is not as well defined by the present experiments as is the isomer yield ratio.

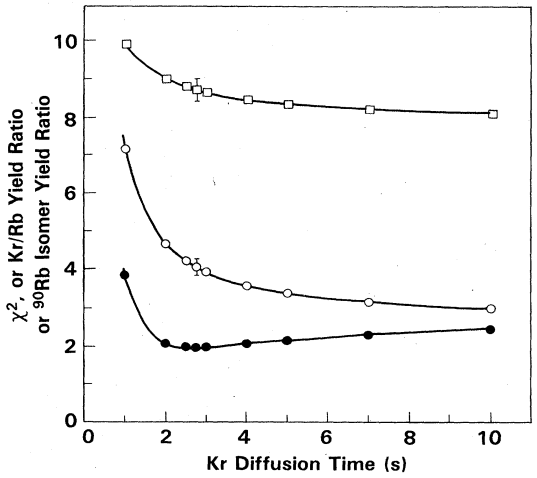

FIG. 7. ^{90}Rb isomer yield ratio (□), Kr independent yield/Rb independent yield (○), and chi-square per degree of freedom (●) from least square fit of isomer yield ratio versus ion collection time data plotted versus Kr diffusion time. Statistical uncertainties are shown on isomer yield ratio and Kr/Rb yield ratio at Kr diffusion time giving the minimum χ_ν^2.

The uncertainty given above for the isomer yield ratio is the statistical uncertainty from the least square fitting program. Uncertainties associated with the Rb and Kr diffusion rate constants are not included. It is also possible that our diffusion and decay model is oversimplified. To estimate limits for higher confidence, one can do an eyeball extrapolation of the data in Fig. 5 and obtain an isomer yield ratio ranging from 7 to 10. It is possible that ^{90}Rb^m has a larger fraction of its beta spectrum below the discriminator than ^{90}Rb^g. A correction for this effect would increase the isomer yield ratio. Although it is difficult to estimate the systematic uncertainties rigorously, we believe that a conservative estimate gives the experimental isomer yield ratio as 8.7 ± 1.0. This ratio is one of the largest ever measured for a low energy fission process.

DISCUSSION

Isomer yield ratios are of interest to applied problems as well as for their use in determining angular momentum of fission fragments. Fission yield data are needed for reactor design for problems such as decay heat, fission product inventory, reactivity, burnup, and delayed neutron abundances. Fission yield compilations have included isomer yield data when available, but generally they have had to use some model calculation to estimate isomer yields due to the lack of data. In particular, the ENDF/B-V compilation[28] uses a model developed by Madland and England.[29] This model assumes that fission fragments are formed with an angular momentum density distribution $P(J)$ characterized by a single parameter,

$J_{\rm rms}=\langle J(J+1)\rangle^{1/2}$.

$$P(J)=P_0(2J+1)\exp[-(J+\tfrac{1}{2})^2/J_{\rm rms}^2]\ . \quad (8)$$

The parameter $J_{\rm rms}$ is assumed to be constant for all fragment masses in the neutron induced fission of actinides. However $J_{\rm rms}$ is allowed to vary with incident neutron energy. This model predicts that isomer yield ratios will depend on the isomer spins, but all isomers with the same spin combination will have the same isomer yield ratio. For the particular spin combination for ^{90}Rb ($J_m=3$, $J_g=0$), this model predicts the highest possible isomer yield ratio of 9.0 which is in excellent agreement with our experimental result.

The model predicts an isomer yield ratio of 4.3 for the spin combination ($J_m=4$, $J_g=1$) which was ascribed to ^{90}Rb earlier.[21] Thus one is tempted to justify the present spin assignment on the basis of the agreement between the experimental isomer yield ratio and the model calculation. However, the model disagrees with experimental values by a factor of 2 in many cases and by a factor of 30 in a recent measurement on ^{148}Pr.[30] Even the assumption that isomers with the same spin combinations have the same isomer yield ratio has been disproven by the measurements on ^{133}Xe and ^{135}Xe by Ford *et al.*[17] where the isomer yield ratios differed by about a factor of 2 for the spins ($J_m=\frac{11}{2}$, $J_g=\frac{3}{2}$). One must be cautious in applying the results of this model.

A statistical model has been proposed by Ford *et al.*[17] to calculate the average angular momentum from knowledge of the isomer yield ratio. This model takes into account nuclear level densities as a function of energy, angular momentum, and parity. It thus allows for variations of isomer yield ratios even for isomers with the same spin combinations. The main feature which distinguishes this model from other statistical calculations is the use of combinatorially calculated level densities. It uses single-particle states in a spherical Woods-Saxon potential as discussed previously.[31] The details of the model and its application to the isomer yield ratios of ^{131}Te, ^{133}Te, ^{133}Xe, and ^{135}Xe are given in Ref. 17.

We have applied the Ford statistical model to ^{90}Rb. The combinatorially determined level density is based on excitation of the 9 protons in the $2p\frac{3}{2}^+$ and $1f\frac{5}{2}^-$ levels and of the 13 neutrons in the $1g\frac{9}{2}^+$ and $2d\frac{5}{2}^+$ levels. All levels between the proton closed shells at $Z=28$ and $Z=50$ and the neutron closed shells at $N=40$ and $N=82$ are included. The calculated level density is weighted by the probability that a state is occupied. The occupation probability is assumed to be proportional to $\exp(-\beta E-\lambda J)$ where β and λ are adjustable parameters. If one chooses particular values of β and λ, one defines the initial probability distribution for excited states of ^{90}Rb. These states then deexcite by gamma emission until one or the other isomeric state is reached. Previous work has shown that the isomer yield ratio and average angular momentum are insensitive to the initial energy distribution.[17] The value of β was chosen for consistency with measurements of average gamma-ray energy and average number of gamma rays emitted for typical fission products. Calculations were done with β fixed at 1 and λ set to various values from 0 to +0.28. For each value of λ, the program calculates several properties for the nuclide and its decay. These quantities for ^{90}Rb are listed in Table II for the λ value corresponding to the experimental isomer yield ratio. Also given in Table II are the same quantities for ^{131,133}Te and ^{133,135}Xe for thermal neutron fission of ^{235}U taken from Ref. 17.

The calculated calibration curves of average J value versus isomer yield ratio are given in Fig. 8 for ^{90}Rb and for the Te and Xe isomers. Even though the ^{131,133}Te and ^{133,135}Xe isomer pairs all have the same spin/parity combinations of $\frac{11}{2}^-$ and $\frac{3}{2}^+$, there are distinct differences in their calibration curves due to their different level densities. The ^{90}Rb has a completely different calibration curve resulting from its different spin combination of 3^- and 0^- (this effect would also be expected from Madland and England's model). However, the average angular momentum deduced from the calibration curves are similar for ^{90}Rb and the Te, Xe isomers as shown in Table II. Figure 8 also shows the calibration curve for ^{90}Rb with

TABLE II. Results of statistical model calculation for products from thermal neutron fission of ^{235}U.

	^{90}Rb	^{131}Te	^{133}Te	^{133}Xe	^{135}Xe
J_m/J_g	3/0	$\frac{11}{2}/\frac{3}{2}$	$\frac{11}{2}/\frac{3}{2}$	$\frac{11}{2}/\frac{3}{2}$	$\frac{11}{2}/\frac{3}{2}$
Experimental isomer ratio	8.7	1.91	1.31	2.85	1.77
λ	0.116	0.091	0.104	0.060	0.106
Average energy (MeV)	3.95	2.51	1.76	3.24	2.33
$\langle J\rangle$	4.53	5.63	4.66	6.83	5.45
$J_{\rm rms}$	5.74	6.95	5.80	8.30	6.75
Fraction of gammas with $L>1$	0.152	0.126	0.131	0.127	0.131
Energy/gamma	1.44	0.72	0.68	0.75	0.69
No. of gammas per fission product	2.70	3.25	2.25	4.07	2.84

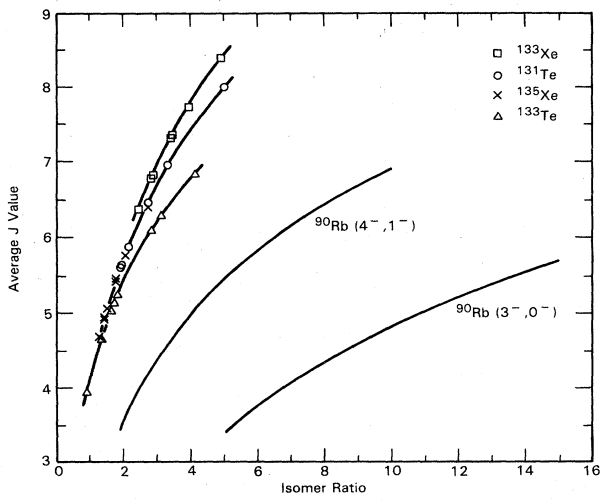

FIG. 8. Calibration curves of average J value versus isomer yield ratio from statistical model calculation. The curve for ^{90}Rb with known spin/parities of 3^- and 0^-, the curve for ^{90}Rb with assumed spin/parities of 4^- and 1^-, and the family of curves for ^{131,133}Te and ^{133,135}Xe all with spin/parities of $\frac{11}{2}^-$ and $\frac{3}{2}^+$ are shown. Data points show location of experimentally measured isomer yield ratios.

the assumption of 4^- and 1^- for the spins and parities of the two isomers. This curve is included to illustrate the sensitivity of the calculation to changes in spin/parity for a given nuclide. It should be emphasized that the statistical model used here treats the fission products only after all neutron evaporation has taken place, i.e., any angular momentum removed by neutron evaporation from the primary fission fragments is not taken into account.

The work of Wilhelmy *et al.*[7] on population of ground state rotational bands of ^{252}Cf fragments indicated that fragments in the light mass peak had lower angular momenta than fragments in the heavy mass peak. The isomer yield ratio data of Bocquet *et al.*[19] also show the trend of lower angular momenta for fragments in the light mass peak. However there are discrepancies between the J values measured by these two techniques, as well as discrepancies with the trends of J value versus mass number calculated by the theoretical model of Zielinska-Pfabe and Dietrich.[4] Our deduced J value for ^{90}Rb is about one unit lower than the average for the Te and Xe isomers, but the range of J values for the Te and Xe isomers is broad enough to bracket the ^{90}Rb value. It appears that variations of angular momentum due to characteristics of individual fission products are comparable to the variations between light and heavy mass regions.

The only previous measurement of the isomer yield ratio of ^{90}Rb was done by Aumann and Weismann[32] for the spontaneous fission of ^{252}Cf. For low excitation energy fission, one does not expect much variation of the isomer yield ratio with changes in the fissioning nucleus.[11,16,17] Thus it is expected that the ^{90}Rb isomer yield ratios of thermal neutron fission of ^{235}U and spontaneous fission of ^{252}Cf should be comparable. Aumann and Weismann obtained a lower limit for the isomer yield ratio of >3.5. They deduced a $J_{\rm rms}$ of >6.2 which is close to our value of 5.7 but their analysis assumed 4^- and 1^- for the spin/parity of the ^{90}Rb isomers. Our calculation for spin/parity 3^- and 0^- with their limit for the isomer yield ratio gives a $J_{\rm rms}$ of >4.0. Because the ^{252}Cf result is a lower limit, the comparison with our ^{235}U result is not very meaningful.

CONCLUSIONS

We have demonstrated a new technique for measuring isomer yield ratios and have presented the results for ^{90}Rb from thermal neutron fission of ^{235}U. As shown in Fig. 5, the apparent isomer yield ratio is strongly dependent on the ion collection time. Collection times of less than 0.1 of the precursor half-life are essential for eliminating interferences from beta decay of the precursor. The conversion of isomer yield ratios to average angular momentum was performed via a statistical model using level densities calculated by combinatorial methods for single particle states near the Fermi surface.[17] Although our experimental isomer yield ratio is very large (8.7 ± 1.0), the resulting angular momentum of the excited fission product ^{90}Rb is similar to the angular momentum deduced for several other fission products.

Only about 10% of the 191 isomers listed in the Japanese Nuclear Data Library of Fission Products have measurements of isomer yield ratios.[33] The present technique has the potential for measuring 26 additional isomer yield ratios. The technique uses a pulsed reactor and an on-line mass spectrometer with a chemically selective ion source. A positive surface ionization source could be used for ^{138}Cs and $^{116-130}$In. A negative ion source could be used for ^{84}Br and $^{132-134,136}$I. A plasma ion source with added CF_4 gas could produce molecular fluoride ions of $^{96-98,100}YF_2^+$ and $^{146}LaF_2^+$. Measurement of isomer yield ratios for many of these fission products would have a significant impact on our understanding of the role of angular momentum in nuclear fission.

This work was supported by the U.S. Department of Energy/Office of Basic Energy Research under Contract DE-AC06-76RL0 1830.

[1]V. M. Strutinsky, Zh. Eksp. Teor. Fiz. **37**, 861 (1959) [Sov. Phys.—JETP **10**, 613 (1960)].
[2]J. R. Nix and W. J. Swiatecki, Nucl. Phys. **71**, 1 (1965).
[3]J. O. Rasmussen, W. Norenberg, and H. J. Mang, Nucl. Phys. **A136**, 465 (1969).
[4]M. Zielinska-Pfabe and K. Dietrich, Phys. Lett. **49B**, 123 (1974).
[5]P. Fong, *Proceedings of the International Symposium on the Physics and Chemistry of Fission, Julich, 1979* (International Atomic Energy Agency, Vienna, 1980), Vol. II, p. 373.
[6]D. De Frenne, B. Proot, H. Thierens. P. De Gelder, E. Jacobs, and A. De Clercq, Phys. Rev. C **29**, 1777 (1984).
[7]J. B. Wilhelmy, E. Cheifetz, R. C. Jared, S. G. Thompson, H. R. Bowman, and J. O. Rasmussen, Phys. Rev. C **5**, 2041

(1972).
[8]F. Pleasonton, R. L. Ferguson, and H. W. Schmitt, Phys. Rev. C **6**, 1023 (1972).
[9]M. M. Hoffman, Phys. Rev. **133**, B714 (1964).
[10]P. Armbruster, H. Labus, and K. Reichelt, Z. Naturforsch. **26a**, 512 (1971).
[11]D. C. Aumann, W. Guckel, E. Nirschl, and H. Zeising, Phys. Rev. C **16**, 254 (1977).
[12]M. Weis and H. O. Denschlag, J. Inorg. Nucl. Chem. **43**, 437 (1981).
[13]S. S. Hsu, J. T. Lin, C. M. Yang, and Y. W. Yu, Phys. Rev. C **24**, 523 (1981).
[14]T. Datta, S. P. Dange, A. G. C. Nair, S. Prakash, and M. V. Ramaniah, Phys. Rev. C **25**, 358 (1982).
[15]H. Thierens, B. Proot, D. De Frenne, and E. Jacobs, Phys. Rev. C **25**, 1546 (1982).
[16]I. Fujiwara, N. Imanishi, and T. Nishi, J. Phys. Soc. Jpn. **51**, 1713 (1982).
[17]G. P. Ford, K. Wolfsberg, and B. R. Erdal, Phys. Rev. C **30**, 195 (1984).
[18]H. O. Denschlag, H. Braun, W. Faubel, G. Fischbach, H. Meixler, G. Paffrath, W. Porsch, M. Weis, H. Schrader, G. Siegert, J. Blachot, Z. B. Alfassi, H. N. Erten, T. Izak-Biran, T. Tamai, A. C. Wahl, and K. Wolfsberg, *Proceedings of the International Symposium on the Physics and Chemistry of Fission, Julich, 1979* (International Atomic Energy Agency, Vienna, 1980) Vol. II, p. 153.
[19]J. P. Bocquet, F. Schussler, E. Monnand, and K. Sistemich, *Proceedings of the International Symposium on the Physics and Chemistry of Fission, Julich, 1979* (International Atomic Energy Agency, Vienna, 1980), Vol. II, p. 179.
[20]J. J. Stoffel(s), Nucl. Instrum. Methods **119**, 251 (1974).
[21]H. Huang, B. P. Pathak, R. Iafigliola, L. Lessard, and J. K. P. Lee, Z. Phys. A **282**, 285 (1977).
[22]C. Ekstrom, L. Robertsson, G. Wannberg, and J. Heinemeier, Phys. Scr. **19**, 516 (1979).
[23]W. L. Talbert, Jr., F. K. Wohn, L. J. Alquist, and C. L. Duke, Phys. Rev. C **23**, 1726 (1981).
[24]F. M. Mann, M. Schreiber, R. E. Schenter, and T. R. England, Nucl. Sci. Eng. **87**, 418 (1984).
[25]B. F. Rider, General Electric Company Report NEDO-12154-3(C), 1981.
[26]F. K. Wohn, K. D. Wunsch, H. Wollnik, R. Decker, G. Jung, E. Koglin, and G. Siegert, Phys. Rev. C **17**, 2185 (1978).
[27]I. Amarel, R. Bernas, J. Chaumont, R. Foucher, J. Jastrzebski, A. Johnson, R. Klapisch, and J. Teillac, Ark. Fys. **36**, 77 (1967).
[28]R. Kinsey, National Nuclear Data Center, Brookhaven National Laboratory, ENDF/B Summary Documentation BNL-NCS-17541 (ENDF-201), 3rd ed. (ENDF/B-V), 1979.
[29]D. G. Madland and T. R. England, Nucl. Sci. Eng. **64**, 859 (1977).
[30]C. Chung, L.-J. Yuan, and W. B. Walters, Z. Phys. A **319**, 295 (1984).
[31]G. P. Ford, Nucl. Sci. Eng. **66**, 334 (1978).
[32]D. C. Aumann and D. Weismann, J. Inorg. Nucl. Chem. **40**, 1611 (1978).
[33]K. Tasaka, H. Ihara, M. Akiyama, T. Yoshida, Z. Matumoto, and R. Nakasima, Japanese Nuclear Data Committee Report No. JAERI 1287, 1983.